Controlling protein adsorption on graphene for cryo-EM using low-energy hydrogen plasmas

Christopher J. Russo[1] and Lori A. Passmore[1]

[1]Medical Research Council Laboratory of Molecular Biology, Cambridge CB2 0QH, UK

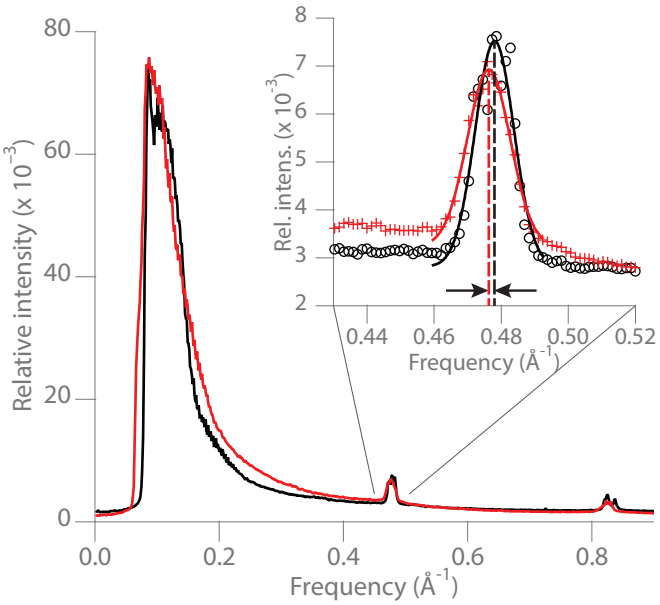

Supplementary Figure 1 | Azimuthal integral intensity plots from selected area diffractograms. Plots are azimuthally integrated diffractograms taken before and after 80 s hydrogen plasma treatment used to measure change in lattice constant vis a vis conversion to graphane. The difference in 0–110 peak position, shown with arrows, is –1.7 x 10^{-3} Å^{-1} which corresponds to a shift of –0.4 % in lattice constant. This is less than the precision of the measurement from sample to sample, which is limited by the variation in lattice constant (≅0.9%) due to stretching of the graphene layer on the grid. Previous studies of graphane formation showed that the lattice constant decreases by ≅5% upon full conversion to graphane[15].

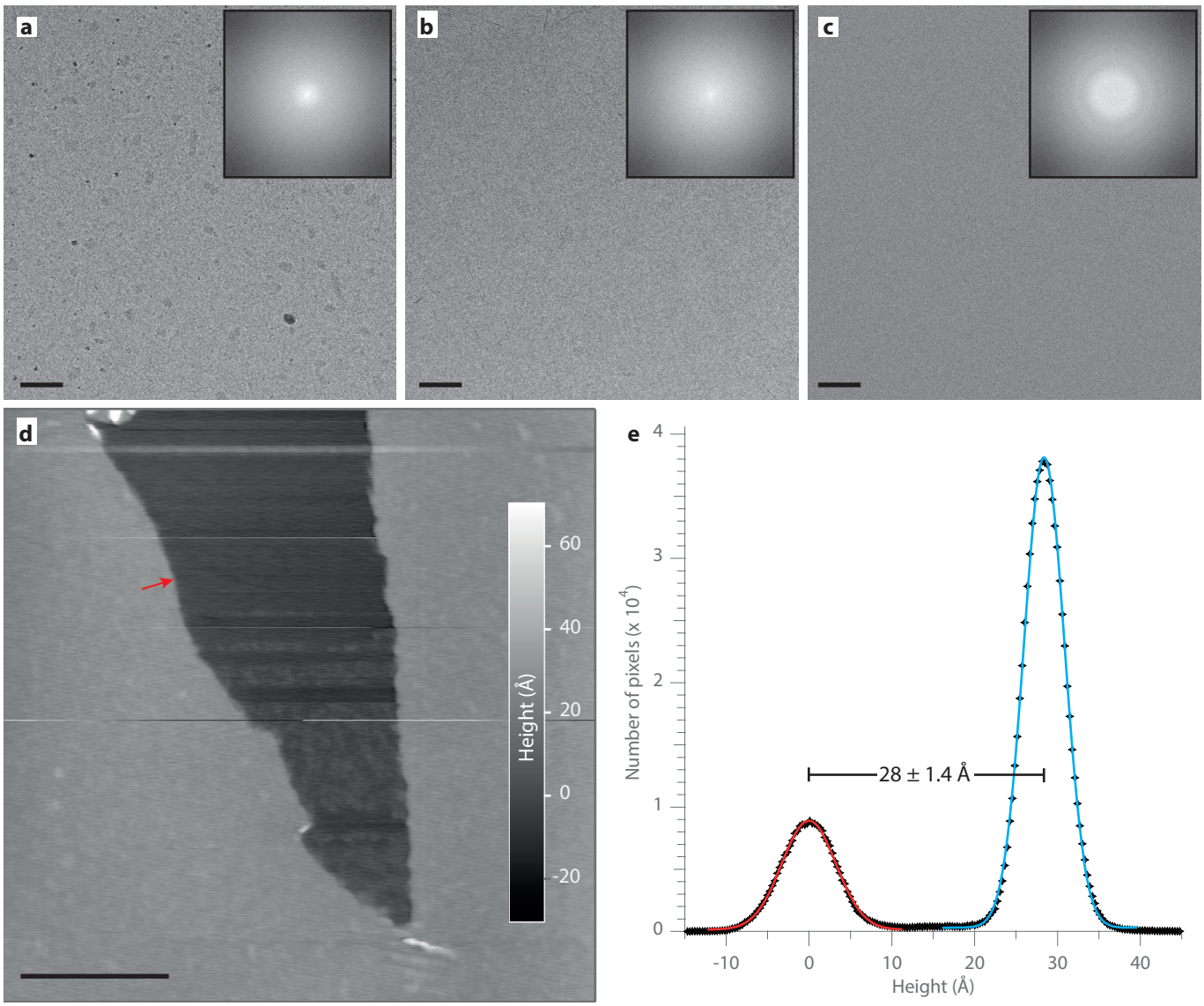

Supplementary Figure 2 | Low-dose images of carbon substrates.
Panel **a** shows untreated graphene, panel **b** is the same sample as **a** after 30 second hydrogen plasma treatment. Panel **c** shows 28 Å thick amorphous carbon for comparison. Insets are the power spectra (FFTs) of each image, reduced to $(1024\ px)^2$, and scale bars are all 2000 Å. Panel **d** is a contact mode atomic force microscopy (AFM) topography image of the edge of the carbon layer from **c** on a mica substrate, which was used to measure the thickness of the carbon layer accurately (scale bar is 5000 Å). Arrow points to the edge of the cleaved carbon layer on the mica substrate. Panel **e** contains a histogram of the height values from **d**, with Gaussian fits to determine the thickness. The smaller red peak is the height of the mica substrate and the larger blue peak is the height on the amorphous carbon layer, and the difference is 28 ± 1.4 Å.

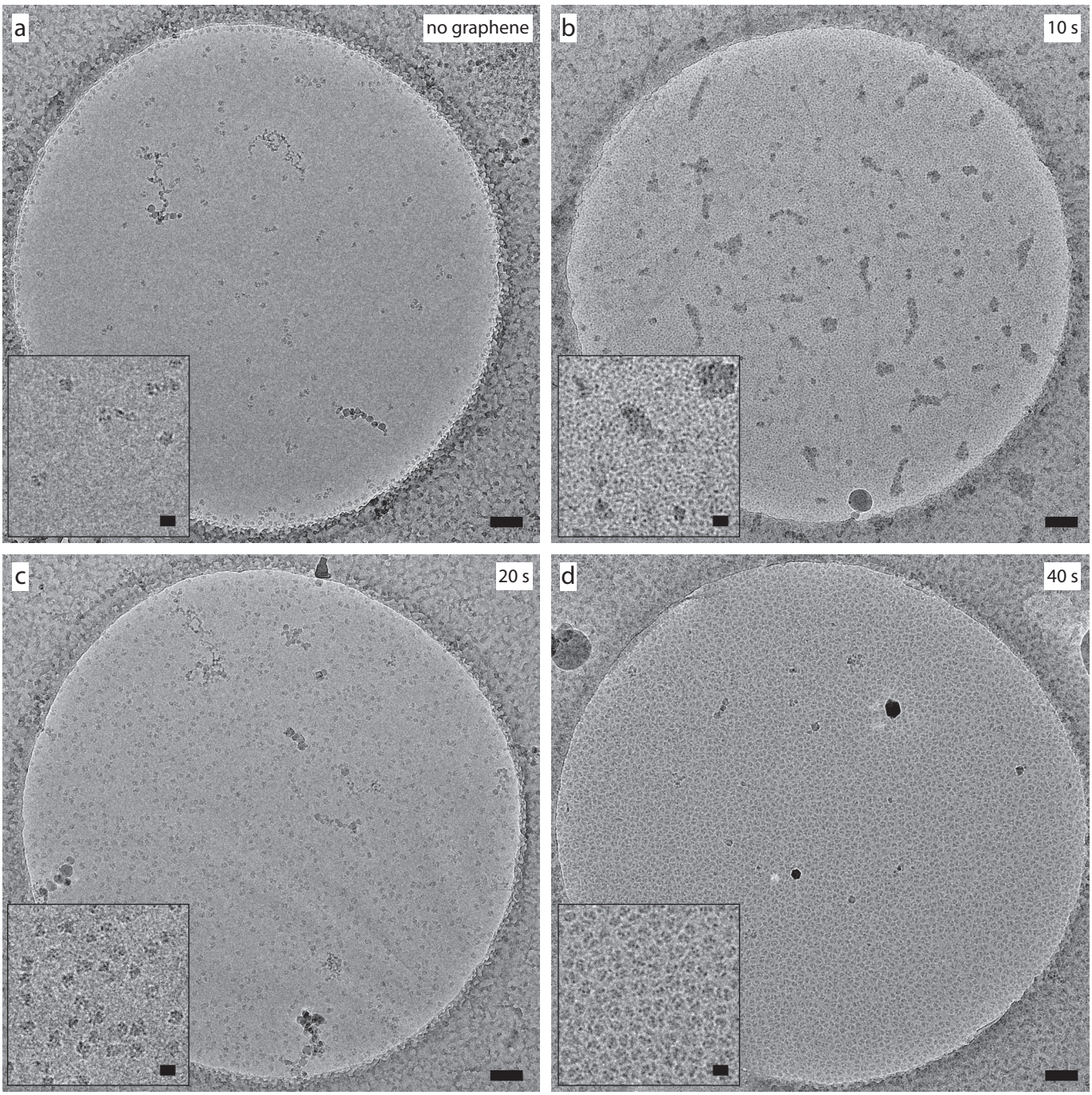

Supplementary Figure 3 | Dose dependent adsorption of ribosomes on hydrogen plasma treated graphene.
Panels **a**-**d** show electron micrographs of 70S ribosomes in vitrified ice at 80 K. Panel **a** is a standard Quantifoil grid treated with a 10 s hydrogen plasma dose. Panels **b**-**d** are Quantifoil grids covered with monolayer graphene, and treated with 10, 20 and 40 s of hydrogen plasma, respectively. All other blotting and vitrification conditions are the same for all four samples. Insets are enlargements of selected regions from each image, showing the typical distribution of particles. Scale bars are 1000 Å for main images and 200 Å for insets.

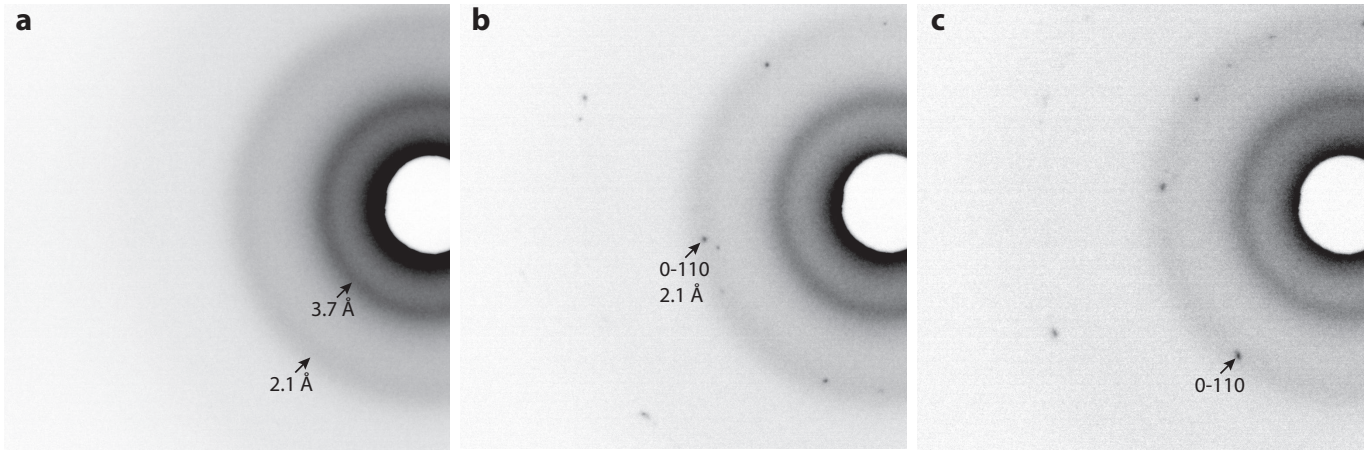

Supplementary Figure 4 | Diffractograms of ribosomes in ice.
Panel **a** shows the selected area diffraction pattern from the unsupported ice in **Fig. 2a**, where the first two diffuse Debye-Scherrer rings for amorphous ice at 3.70 Å and 2.14 Å are indicated with arrows[3]. The white disk at the center is the shadow of the primary beam stop, a homemade platinum ball on a wire. Panel **b** shows the diffraction pattern for the ribosomes in ice on suspended graphene (20 s dose) in **Fig. 2a**, where the 0–110 reflection at 2.14 Å of the monolayer graphene is indicated, and sets the magnification scale for all three diffractograms. Similarly, panel **c** shows the diffractogram for the ribosomes in ice on suspended graphene (40 s dose) for **Fig. 2a**, with the 0–110 peak indicated. Additional diffraction peaks are from small contaminant ice crystals on the surface of the thin film, which are visible in the micrographs. The camera length for each diffractogram is the same, nominally 47 cm.

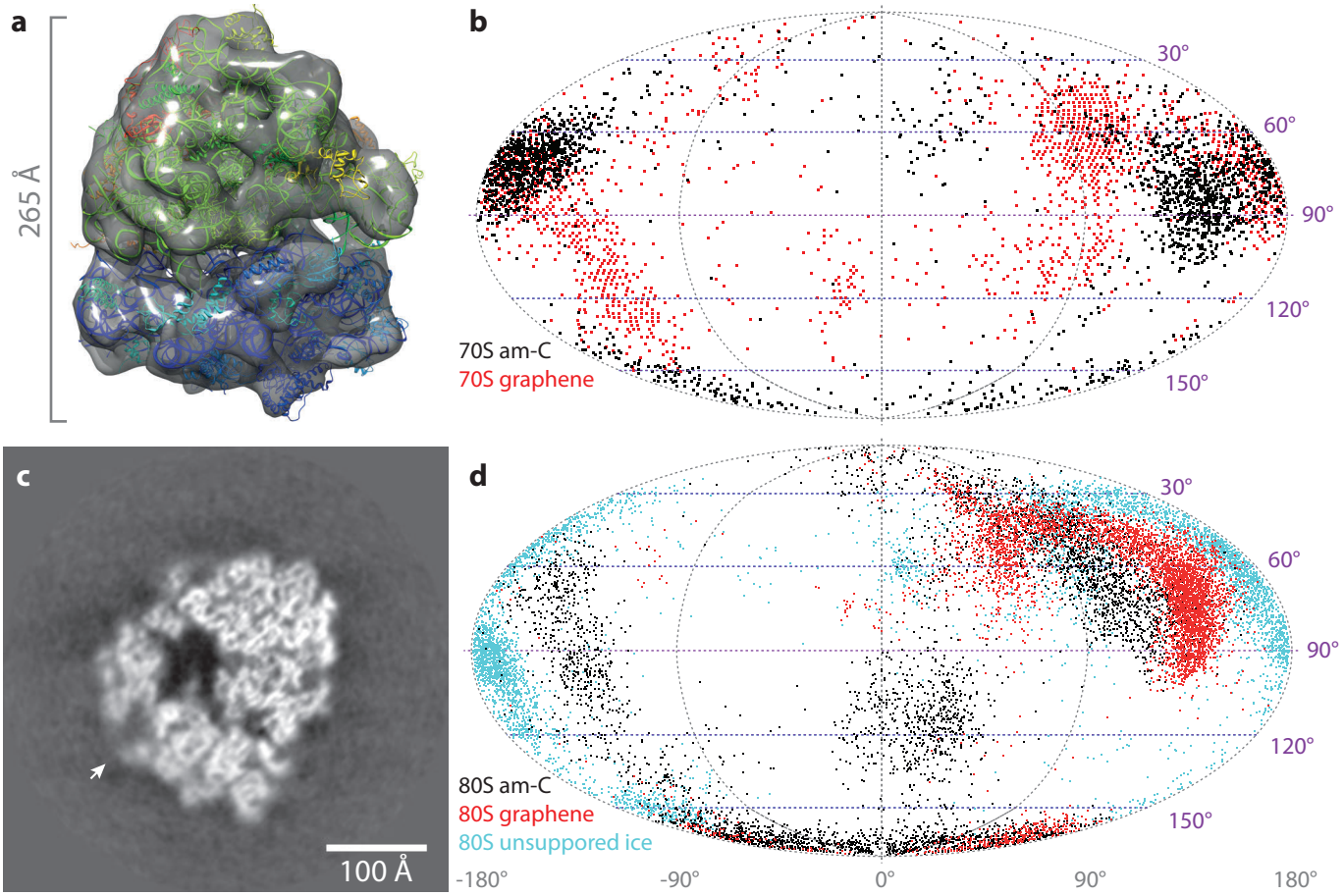

Supplementary Figure 5 | Analysis of ribosome structural data on hydrogen plasma treated graphene. Panel **a** shows a 3D rendering of the density map of the *T. thermophilus* 70S ribosome, reconstructed to 19 Å from three micrographs of particles on graphene. The overlaid ribbon diagram is the rigid-body fit of the crystal structure to the map. Panel **b** is an equal area projection map of the orientation angles of the 2061 ribosomes relative to a graphene substrate (red dots) and an am-C substrate (black dots). Image **c** is a 1.3 Å slice through the unsharpened density map of the *S. cerevisiae* 80S ribosome reconstructed to 5.0 Å on graphene. Blurring of the 40S subunit (arrow) is due to conformational heterogeneity of the sample; this and non-optimal coverage of orientations in Fourier space limit the resolution of the map. Panel **d** is the equal area projection map of the orientations of 10000 80S ribosomes (a randomly selected subset for plotting) from each of three different supports: in ice without a support layer (blue dots), on graphene (red dots) and on am-C (black dots).

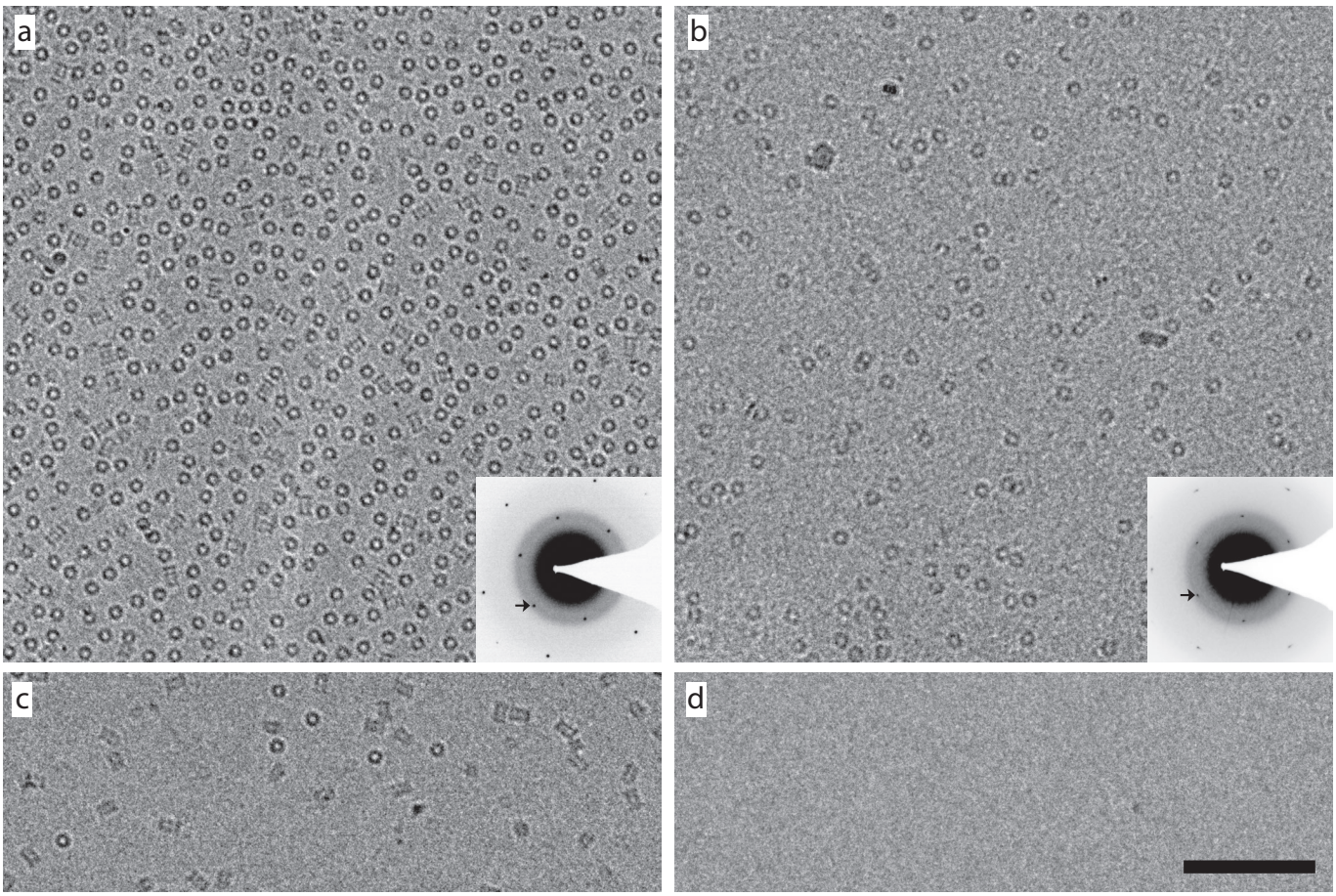

Supplementary Figure 6 | Specific adsorption of proteins to hydrogen plasma treated graphene. Left column comprises electron micrographs of human 20S proteasome in vitreous ice. Panel **a** shows molecules on graphene treated with 40 s of hydrogen plasma and panel **c** shows molecules in ice an adjacent region of the same grid without graphene. Right column (**b** & **d**) shows the same for horse spleen apoferritin. Insets are the electron diffractograms from the regions imaged, with arrows pointing to the 0-110 graphene reflection. The increase in surface particle density on the graphene support is 6-fold for the proteasome and is likely saturated, and >500-fold for apoferritin. Scale bar is 1000 Å and magnification is the same for all micrographs.

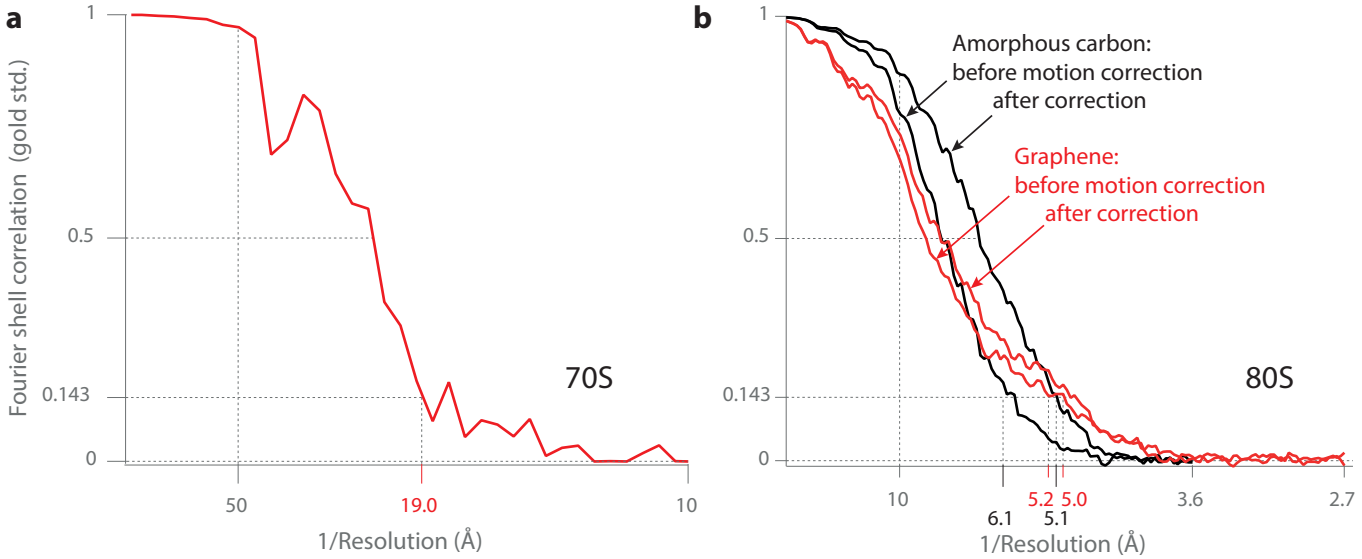

Supplementary Figure 7 | Fourier shell correlation coefficients.
Calculated for the 70S (**a**) and 80S (**b**) ribosomes using the reconstructed electron density map refined from two random halves of the dataset, keeping each separate through the reconstruction process ("gold standard")[30,35]. Using the 0.143 criterion[36], the resolution for the 70S map from 2061 particles on graphene using three micrographs was 1/19.0 Å. The resolution of the 80S map from 20,050 particles on graphene was 5.2 Å, and showed little improvement to 5.0 Å, with motion correction (**b**, red curves). We compare this to a reconstruction using the same number of particles chosen at random from a previously published dataset on the same ribosome sample where the resolution is 6.1 Å before motion correction and 5.1 Å after motion correction (black curves)[2].

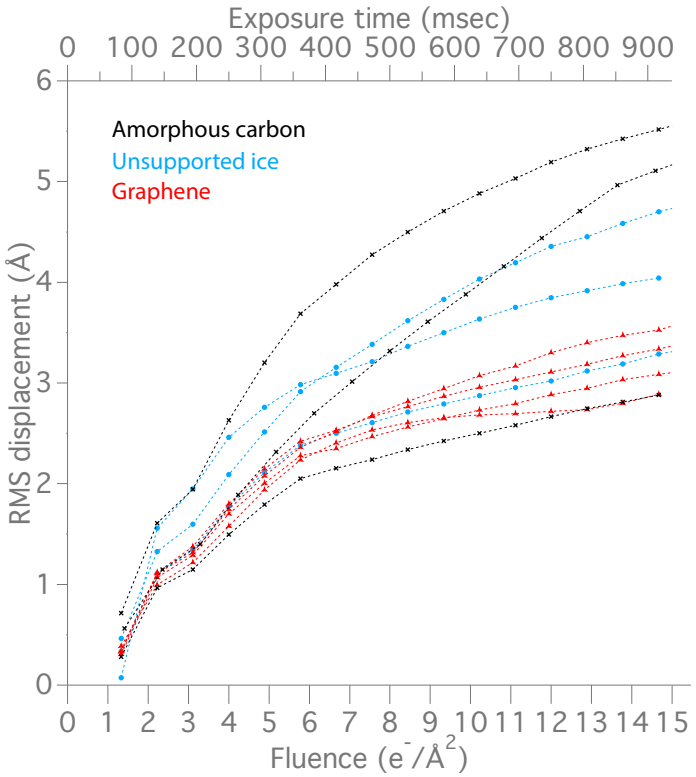

Supplementary Figure 8 | Speed plots of ribosomes on various substrates.
The root mean squared (RMS) displacement from the initial position of 80S ribosomes during electron beam irradiation is measured for ten grids with three different substrates as detailed in the methods: amorphous carbon, unsupported ice and hydrogen plasma treated graphene. Data is the same as contained in **Fig. 3** except plotted together to facilitate comparison. Each curve is calculated from thousands of particles on a single grid. Electron fluence for all experiments was 16 $e^-/Å^2/s$ and energy was 300 keV.

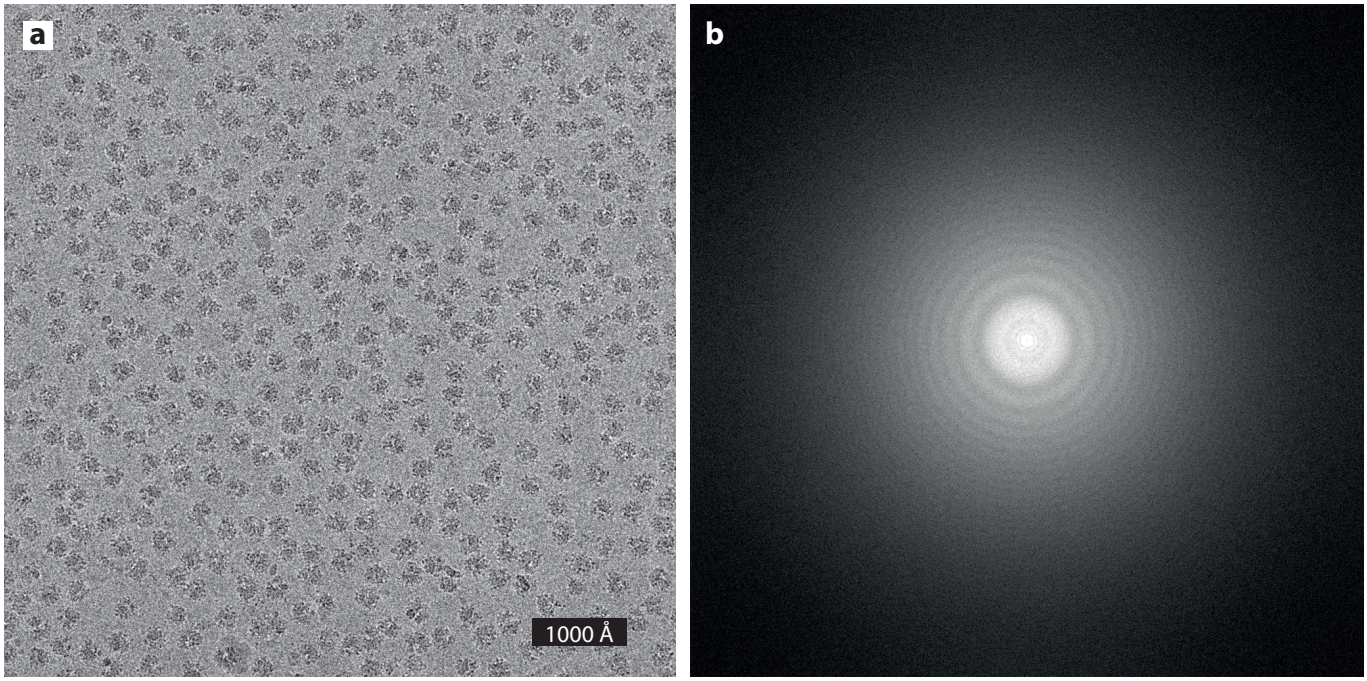

Supplementary Figure 9 | Electron micrograph of 80S ribosomes on graphene.
Panel **a** is a typical micrograph of 80S ribosomes on hydrogen plasma treated graphene. Image was down sampled from 4096 x 4096 pixels (1.7 Å / px) x 16 bits of native resolution to 1024 x 1024 pixels and intensity was scaled to an 8 bit window comprising ± 3σ about the mean intensity value. Panel **b** is the power spectrum of **a**, showing the phase contrast rings from the ribosomes alone, as the graphene does not contribute to spectral frequencies in this range. The focus value for this micrograph was –2.7 μm.

Supplementary Table 1 | Radiation-induced particle speed on various substrates (**Fig. 3**).

Substrate	Phase 1		χ^2	Phase 2		χ^2
Unsupported ice	8.0 ± 2.1 Å/s	0.50 ± 0.13 Å/e$^-$/Å^2	0.79	2.2 ± 0.8 Å/s	0.14 ± 0.06 Å/e$^-$/Å^2	0.076
Amorphous carbon	7.5 ± 2.1 Å/s	0.47 ± 0.13 Å/e$^-$/Å^2	0.16	2.8 ± 0.1 Å/s	0.18 ± 0.06 Å/e$^-$/Å^2	0.12
Graphene	6.6 ± 2.1 Å/s	0.41 ± 0.13 Å/e$^-$/Å^2	0.26	1.5 ± 0.8 Å/s	0.092 ± 0.06 Å/e$^-$/Å^2	0.03

Supplementary Note 1 | Calculation of graphene-water interfacial energy.
For a liquid droplet in a gas environment on a solid surface, the liquid-solid interfacial energy, *W*, is related to the equilibrium contact angle between the droplet and the surface, by the Young-Dupré equation:

$$W = \gamma_w(1 + cos\ \theta)$$

where γ_w is the water surface tension, 72 mJ/m^2[37]. Using the contact angle values from the as-grown graphene sample ($\theta_{gr} = 91 \pm 0.5°$) and the saturation value from the exponential fit to the data, ($\theta_{grh} = 66 \pm 1.3°$) the change in surface energy due to the hydrogen plasma treatment is then just the change in the interfacial energy for the two surfaces:

$$\Delta W = \gamma_w(cos\ \theta_{gr} - cos\ \theta_{grh})$$

which for the values measured is –0.19 ± 0.02 eV/nm^2. While the presence of the copper substrate may cause a small reduction in the measured angle for native graphene[38], it will have negligible effect on the change in angle used to calculate the change in interfacial energy as the substrate will have the same effect on all the measurements.

Supplementary Note 2 | Proposed model of hydrogen-induced changes in graphene-water interfacial energy.
The water-graphene interfacial energy is dominated by hydrophobic interactions between water and the non-polar graphene lattice. Adding hydrogen disrupts the ordering of water molecules near the graphene surface and thus increases the entropy until the separation between hydrogens is comparable to the length scale of water coordination near the surface. Hydrophobic interactions are long-range and decay exponentially with a decay constant of ~1 nm in water[18]. Since (1) the change in interfacial energy we measure saturates with the addition of order one hydrogen / nm^2, and (2) the total change in surface energy is of the same order as the hydrophobic interaction in water, we conclude that the hydrogen plasma treatment primarily makes the graphene lattice hydrophilic by adding hydrogen atoms that disrupt the local ordering of water molecules at the graphene-water interface.

SUPPLEMENTARY REFERENCES

37. Israelachvili, J. N. *Intermolecular and Surface Forces*. (Academic Press, 2011).

38. Shih, C.-J. *et al. Phys. Rev. Lett.* **109,** 176101 (2012).